



## ORIGINAL PAPER

**BASIC RED-5 ADSORPTION ON MONTMORILLONITE: FACTORIAL DESIGN, EQUILIBRIUM, KINETIC AND THERMODYNAMIC STUDIES**

Feza GEYIKCI

*Department of Chemical Engineering, Ondokuz Mayıs University, 55139, Samsun, Turkey**\*Corresponding author's e-mail: fezag@omu.edu.tr***ARTICLE INFO****Article history:**

Received 4 July 2019

Accepted 22 June 2020

Available online 5 August 2020

**Keywords:**

Basic Red 5

Isotherm

Kinetic

Factorial design

Montmorillonite

**ABSTRACT**

In this study, the adsorption performance of montmorillonite (MMT) was evaluated by Basic Red-5 adsorption experiments considering the influencing factors (initial BR-5 concentration, dosage, time, pH, and temperature). The surface and structural properties were characterized by FT-IR, XRD, XRF, SEM-EDS, AFM, and BET techniques. The adsorption experiments were carried out by batch mode for the evaluation of isotherm, kinetic, and thermodynamic studies. The results of equilibrium adsorption isotherm were interpreted using different isotherm models. The equilibrium data fitted well with the Langmuir isotherm models, and the maximum adsorption capacity was found as 163.93 mg/g. Adsorption data of the BR-5 onto MMT provide well by pseudo-second-order model ( $R^2=0.999$ ). The  $\Delta H^\circ$ ,  $\Delta S^\circ$  and  $\Delta G^\circ$  values were calculated for the nature of the adsorption process. The analysis of the thermodynamic parameters showed spontaneous, exothermic, and viable adsorption of BR-5 under the investigated experimental conditions. A factorial design was applied to examine the effect of three factors initial concentration of dye (50 and 100 mg/L), time (60 and 120 min.) and dosage (0.05 and 1.00 mg/L) on the adsorption process. According to the results, with high efficient adsorption capacity and compatible surface properties are advantageous to be used for uptake of dyes.

**1. INTRODUCTION**

Dyes are mainly used in the textiles, packed food, tanneries, leather, pharmaceutical industries, pulp and paper, paint, cosmetics, and electroplating industries. More than 100,000 commercial dyes are in use, and the production of dye is estimated to increase at 3 % per year (Sarma et al., 2016; Yeddou-Mezenner, 2010).

Most of the synthetic dyes have a complex aromatic structure, which makes them biodegradable difficult into the environment. The presence of low dye concentrations in the wastewaters caused toxicological and technical problems and environmental pollution. Basic dyes can be applied to wool, silk, and leather (Han et al., 2008). The wastewater of these industries is very colorful and harmful to the environment. Synthetic dyestuffs in the wastewater can prevent photosynthesis.

Furthermore, due to carcinogenic, mutagenic and teratogenic effects, dye contaminated wastewater is considered as a biological threat for the marine environment. Also, this wastewater can cause severe damage to human health by damaging the kidney, liver and brain functions, reproduction, and central nervous system. Azo dyes are toxic because of the presence of toxic amines in the effluent (Hamza et al., 2018; Tahir and Rauf, 2006).

Various techniques are (coagulation, chemical oxidation, membrane separation processes, electrochemical, aerobic and anaerobic microbial degradation) utilized for removal of dyes from wastewaters, but these techniques have some limitations. Adsorption process has been widely applied for the removal of dyes. This process is recognized to be one of the most effective methods for removing dyes from wastewater due to its low cost, insensitivity to toxic substances, ease of operation and no sludge formation (Eren, 2009).

Clay minerals have a unique structure used in many areas. They have been used for the removal of contaminants, delivery of drugs and different active molecules, and to improve mechanical and barrier properties in polymer films. Many researchers have proposed various natural clay minerals in the treatment of wastewater (Eren, 2009; Tahir and Rauf, 2006). MMT is a natural clay group that has nanostructure with a large surface area. It has the layers of two tetrahedral silica sheets sandwiching one octahedral alumina sheet. This crystal cell is generally unstable, and the ions are easier to be replaced by other ions. Therefore, MMT has excellent performance in adsorbing organic/inorganic cations contaminants by the cationic exchange. It has been reported that the abundance of MMT and its low cost has posed them

**Table 1** The chemical composition of MMT.

Compounds	SiO <sub>2</sub>	Al <sub>2</sub> O <sub>3</sub>	Fe <sub>2</sub> O <sub>3</sub>	MgO	K <sub>2</sub> O	CaO	TiO <sub>2</sub>	Na <sub>2</sub> O	MnO	Cr <sub>2</sub> O <sub>3</sub>	P <sub>2</sub> O <sub>5</sub>	Loss on ignition
w %	57.80	17.70	7.90	2.40	1.60	1.50	0.80	0.50	0.30	0.10	<0.10	9.05

a strong candidate as an adsorbent for the removal of dye and heavy metal from wastewater. The relationship between the molecular structure of these dyes and clay minerals has recently been discovered (Ates et al., 2017; Bergaya and Lagaly, 2008; Bujdak, 2006; Huang et al., 2017). The uptake of various cationic dyes on MMT has also been extensively studied, including crystal violet, methylene blue, congo red, malachite green, rhodamine B, etc.

In this work, the use of natural MMT for the adsorption of BR-5 from aqueous solution by batch adsorption is presented. The equilibrium, kinetic and thermodynamic data of the adsorption process were studied to explain the adsorption mechanism of BR-5 molecules onto the MMT. A factorial design is employed to reduce the total number of experiments. The best individual and interactive effects of the adsorption parameters were achieved by the design method.

## 2. MATERIALS AND METHODS

### 2.1. MATERIALS

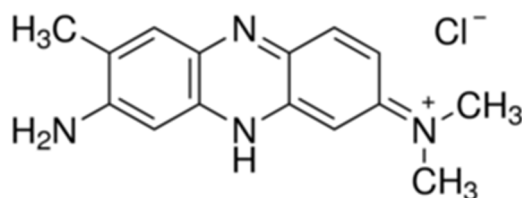
In this study, MMT samples used in the experiments were supplied from Bafra (Samsun) in Turkey. The chemical composition of the MMT was analyzed by XRF and given in Table 1. BET specific surface area of MMT was obtained 73.92 m<sup>2</sup>/g by N<sub>2</sub> adsorption isotherms measured at liquid nitrogen temperature using a Quantchrome Autosorb IQ 2 instrument.

The Fourier transform infrared (FT-IR) spectra of the MMT were recorded in the region 650-4000 cm<sup>-1</sup> on a Perkin Elmer Spectrometer at a resolution of 4 cm<sup>-1</sup>.

XRD analysis of the MMT was carried out with a PHILIPS PW 1710 diffractometer using Cu K $\alpha$  radiation, in the 2 $\theta$  angle range from 2.5° to 70°, with a 0.02 step. FT-IR analysis was also performed with Perkin Elmer Spectrum Spectrometer.

TGA and DTG analysis were carried out on an SDT Q 600 thermal analyzer combined TAS 100 (range 25-500 °C) under oxygen flow (50 mL/min) with a heating rate of 10 °C/min.

The DSC curves were obtained in a calorimeter (model DSC Q20 with RCS90) coupled with a cooling system, both from TA Instruments. A portion of each sample (10 ± 0.5 mg) was loaded in an aluminum pan, and heat flow was measured differentially by comparison to the heat flow of an empty reference pan as a reference. The rate of heating was 10 °C/min between -25 °C and +500 °C under an inert nitrogen atmosphere (N<sub>2</sub>) with a flow rate of 50 mL/min.

**Fig. 1** The chemical structural formula of BR-5.

SEM-EDS analysis carried out on a Jeol Brand JSM-7001FTTLS LV model scanning electron microscope with 12 000x magnification. The images of particles were obtained using the atomic force microscope (AFM). AFM is designed as a portable system by Nanomagnetics Scientific Instruments Company.

The dye used in the experiments was BR-5 (C.I. Basic Red 5, 50040, 3-Amino-7-dimethylamino-2-methylphenazine hydrochloride, Neutral Red) which is widely used as suitable a bioreagent (Fig. 1) for cell culture (Verissimo et al., 2016). The molecular weight of the BR-5 is 288.78 g/mol. BR-5 has great potential as photosensitizers. It is a phenazine dye usually used to stain cells in studies of in vitro cytotoxicity and phototoxicity in cell. Apart from these uses, BR-5 has been described in the literature as an intracellular pH indicator and assay dye. BR-5 gives red color to lysosomes. Also, BR-5 is a component of MacConkey agar and indicates the presence of lactose (Ates et al., 2017; Fotakis and Timbrell, 2006; Mannerström, 2017).

### 2.2. ADSORPTION EXPERIMENTS

The initial BR-5 concentration, pH, dosage, time and temperature were selected as experimental parameters. The BR-5 stock solution (1000 mg/L) was prepared and diluted to different concentrations. Batch experiments were conducted in a thermostatic shaker bath at the different dye concentrations ranging from 20 to 200 mg/L. The effect of pH was analyzed over the pH range of 2 and 8. The pH was measured by WTW 330 pH-meter using with HNO<sub>3</sub> (Merck) and NaOH (Merck) solutions. The samples were continuously mixed with a speed of 175 rpm at 22 °C. At the end of the adsorption period, the suspensions were centrifuged for 10 min at 4500 rpm, and the phases were separated. The concentration of dye remaining in the supernatant was measured with a 1.0 cm light path quartz cells using UV/Vis spectrophotometer (Agilent Technologies Cary 60 UV-Vis) at  $\lambda_{max}$  of 530 nm.

**Table 2** Parameters of the factorial design.

Factor	Symbol	Low Level (-1)	High Level (+1)
Initial Concentration (mg/L)	A	<b>50.00</b>	100.00
Time (min.)	B	<b>60</b>	120
Dosage (g/L)	C	<b>0.05</b>	0.10

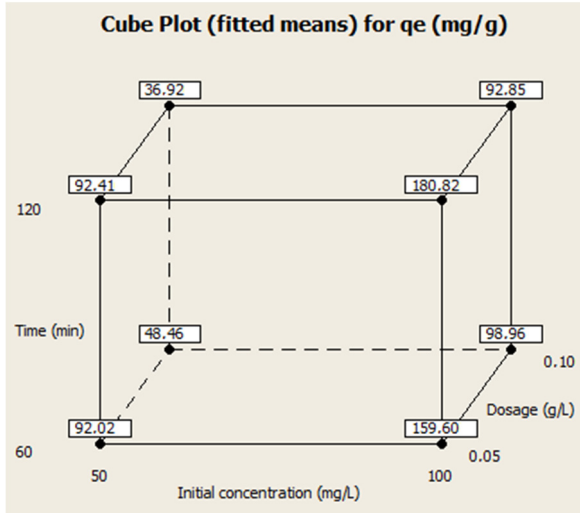


**Fig. 2** Cube plots for  $q_e$ .

The initial concentrations were performed with a considerable interval of BR-5 initial concentrations (20-200 mg/L) at the optimum conditions for 2 h. The equilibrium amount of adsorption  $q_e$  (mg/g) and the amount of adsorption at equilibrium time  $q_t$  (mg/g) were calculated based on the following equations: (Eqs. 1, 2):

$$q_e = \frac{(C_o - C_e)V}{m} \quad (\text{Eq. 1})$$

$$q_t = \frac{(C_o - C_t)V}{m} \quad (\text{Eq. 2})$$

where  $C_o$  (mg/L),  $C_e$  (mg/L), and  $C_t$  (mg/L) are BR-5 concentrations at the initial, equilibrium and time  $t$  (min),  $V$  (mL) are the volumes of the solution, and  $m$  (g) is the weight of MMT.

**2.3. FACTORIAL EXPERIMENTAL DESIGN**

Factorial design was carried out to reduce time, the number of experimental costs and to find a better response. In many experimental studies, the researchers have successfully applied the experimental design (Farooq et al., 2017; Lima et al., 2011). The  $2^3$  factorial experiments were applied, in two levels as high and low. The factors and their two levels were listed in Table 2. The low and high levels of the factors were determined by considering some preliminary experiments. The experiments were carried out by two parallel, and adsorption capacity ( $q_e$ ) was defined as the average of experiments. The results of experiment data were analyzed with the Minitab 16 software, and the main effects and interactions between factors were determined (Gabor et al., 2017; Ponnusami et al., 2007). The cubical diagram for three high and low factors; initial concentration, time and dosage is given in Figure 2.

**3. RESULTS AND DISCUSSION**

**3.1. THE CHARACTERIZATION OF THE MMT**

**3.1.1. FT-IR ANALYSIS**

FT-IR spectra of MMT and MMT/dye composite are shown in Figure 3. The weak broad band that appeared in FTIR spectra of dye-MMT composite at

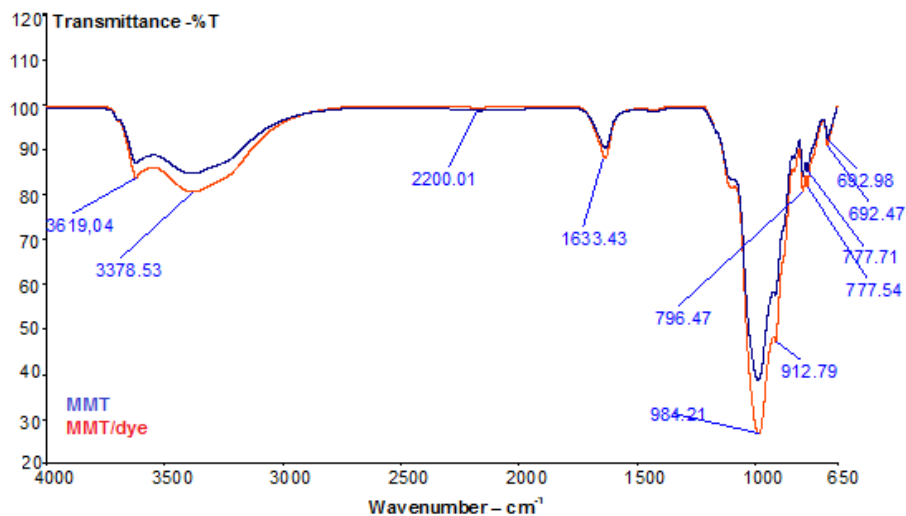


**Fig. 3** FT-IR spectra of MMT and MMT/dye composite.

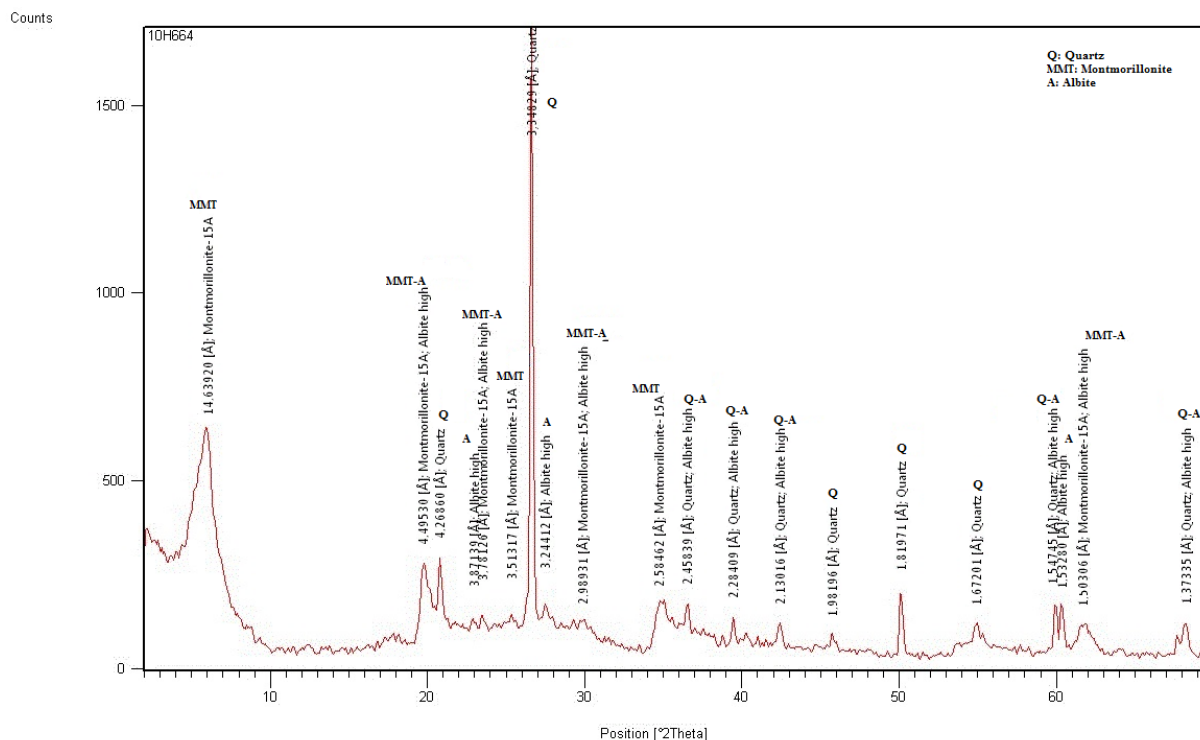


Fig. 4 XRD pattern of MMT-X-ray diffractograms pattern.

around  $2200.01 \text{ cm}^{-1}$  indicates  $\text{N}=\text{C}=\text{N}$  bonds. The bands at  $3619.04$  and  $3378.53 \text{ cm}^{-1}$  are attributed to the O-H stretching vibrations of silanol (Si-OH) groups and H-OH (water belonging to the original MMT structure), respectively. The peaks at  $1633.43$ ,  $984.21$  and  $912.79 \text{ cm}^{-1}$  are due to bending vibration of H-OH, the stretching vibration of Si-O-Si groups of the tetrahedral sheet and Al-O-(OH)-Al, respectively. The peak at  $796.47 \text{ cm}^{-1}$  corresponded to the bending, deformation vibration of Si-O bond and relates to quartz that is identified in the XRD pattern. According to the results of FTIR analysis, this peak can be explained by the presence of amorphous silica in the MMT. For raw MMT and MMT/BR-5 composite, Mg-OH vibration band is observed at  $692.47 \text{ cm}^{-1}$  and  $692.98 \text{ cm}^{-1}$  (Djomgoue et al., 2013; Wu et al., 2011).

### 3.1.2. XRD ANALYSIS

XRD spectrum of the surface functional groups of the MMT is presented in Figure 4. According to XRD analysis, MMT samples have a mineral composition of quartz, feldspar group and amorphous material. The feldspar group contains albite, and the chemical formula is  $\text{NaAlSi}_3\text{O}_8$ . Na is bonded on albite. K is bonded in the interlayer of MMT. SEM-EDS analysis shows that K is observed in MMT. The results were supported by XRF analyses (Gulgonul and Celik, 2018; Wang et al., 2017).

### 3.1.3. THERMOGRAVIMETRIC ANALYSIS

The thermal behaviour and thermogravimetric curve of the MMT are shown in Figure 5. The large peak in the low-temperature region can be attributed to the loss of sorbed water. The form of endothermic

effects can be of double or straightforward character depending on the nature of exchange cations. The MMT with different cations in the interlayer space may have different interlayer distance. If the basal spacing found between  $9.8\text{--}10 \text{ \AA}$  water molecules are adsorbed mainly on the outer surface of the 2:1 phyllosilicates (hydromicas). The basal spacing between  $14.5\text{--}15 \text{ \AA}$  indicates that a second water layer is formed in the interlayer space. The MMT saturated with monovalent cation has only a single thermal dehydration peak. The amount of water is about 7 %, due to the water form of the monolayer in the interlayer space ( $d(001) = 12\text{--}12.6 \text{ \AA}$ ).

In this study, the first endothermic peak at the  $25\text{--}100 \text{ }^\circ\text{C}$  on the DTA curve of the MMT corresponds to the removal of moisture and the interlayer water. The mass loss by was 8.8 % in this temperature range. The escape of the free liquid “sticking” water as a colloid system from the surface is at lower temperatures compared to the interlayer water. The results showed that the decomposition and dehydroxylation process of MMT impurity occurs between the temperature ranges  $27.836\text{--}177.77 \text{ }^\circ\text{C}$  and the mass loss is 9.1106 %. An endothermic peak at the  $350\text{--}500 \text{ }^\circ\text{C}$ , which exhibits a mass loss by 4.0 %, represents desorption of bounded water. Total mass loss is found 14 %, and this result is compatible with the literature (Földvári, 2011). According to the result of DSC analysis, the weight loss with a strong endothermic peak is around  $50 \text{ }^\circ\text{C}$ , and  $-59.2 \text{ mW}$  can mainly show the dehydration of water adsorbed in the interlayer space of MMT. The TG-DTG analysis supports the result of DSC analysis.

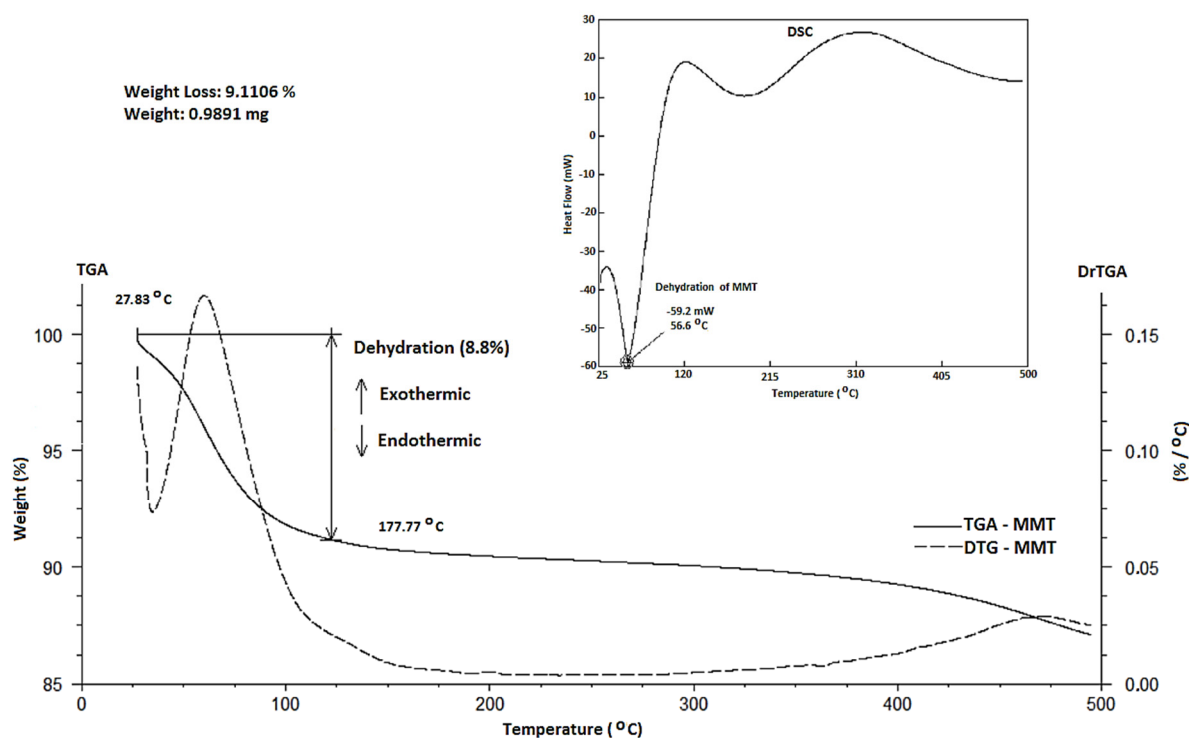


Fig. 5 TG and DTG curves of the MMT.

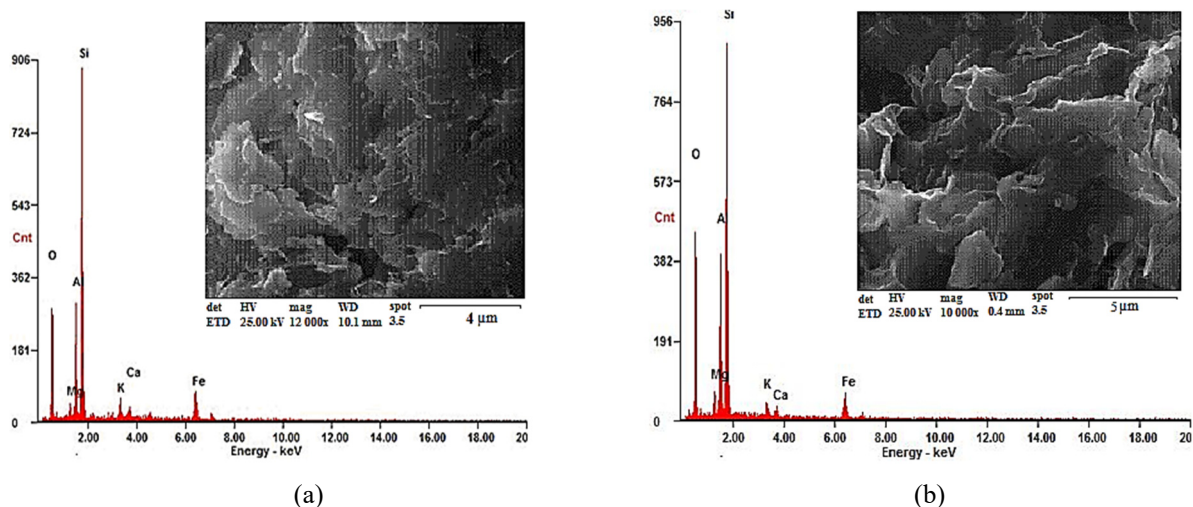


Fig. 6 SEM-EDS analysis of MMT (a) and MMT/BR-5 (b).

3.1.4. SEM AND EDS ANALYSIS

The SEM images and EDS analysis of the MMT and MMT-BR-5 were presented in Figure 6 (a) and (b). The SEM and EDS are uniquely suitable for studying the structure of MMT because they enlarge the display of MMT surfaces as well as bring out the configuration, texture and fabric of clay samples. These figures show that those samples are characterized by the presence of particles having different sizes and specific MMT morphology. EDS measurements of MMT and MMT-BR-5 were carried out to find out the distribution of elements on the sample surface. The composition of elements in MMT

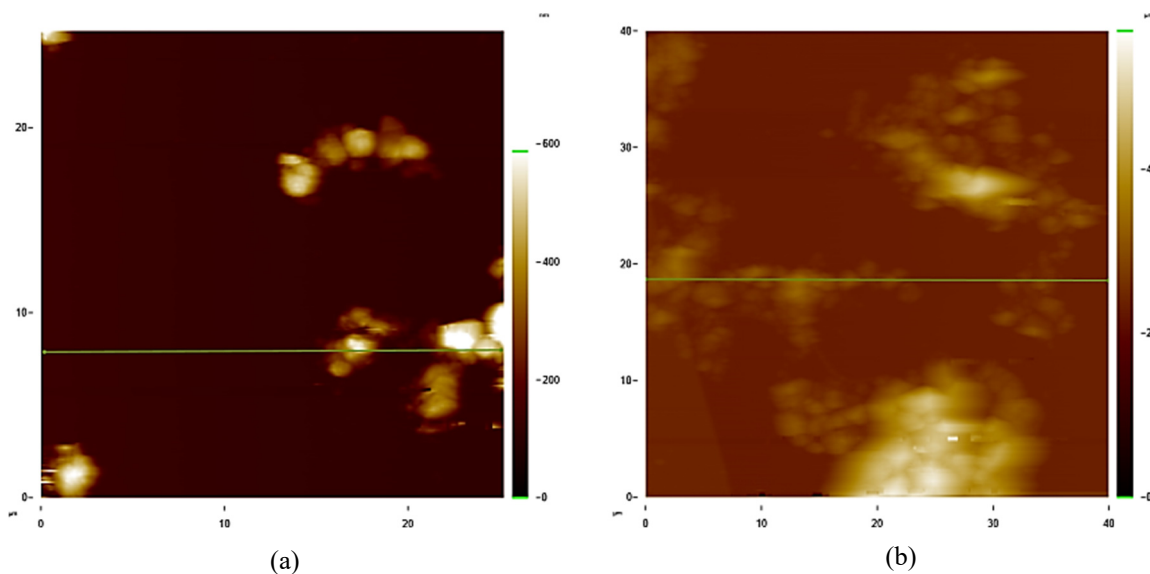
was determined via SEM-EDS instrument (Fig. 6 (a)), and the results are given in Table 3 as percent ratios. According to the obtained results, it is possible to highlight the presence of silicon and aluminum at significant percentages compared to other elements, such as magnesium, iron, potassium and calcium.

3.1.5. ATOMIC FORCE MICROSCOPY (AFM)

The surface morphology of the MMT has been studied by Atomic Force Microscopy in tapping mode. Figure 7 (a) and (b) indicate the BR-5 molecules are organized onto the substrate along with their aggregated structures. Furthermore, the aggregation of

**Table 3** Mass and atomic percentages of elements of the MMT.

Element	O	Mg	Al	Si	K	Ca	Fe
Mass (%)	38.52	1.65	11.49	37.32	2.11	1.32	7.59
Atom (%)	54.07	1.53	9.57	29.84	1.21	0.74	3.05

**Fig. 7** Tapping mode Atomic Force microscopic images of (a) MMT and (b) MMT-BR-5.**Table 4** Surface morphological parameters MMT-BR-5 deposited onto MMT as obtained by Atomic Force Microscopy (tapping mode).

Systems	RMS roughness	Average roughness	Average height	Surface skewness
MMT (a)	0.54 $\mu\text{m}$	0.35 $\mu\text{m}$	5.50 $\mu\text{m}$	2.716 nm
MMT-BR-5 (b)	70.32 nm	34.97 nm	723.19 nm	4.192 nm

particles may be connected with the amount of Basic Red-5 sorbed. In the AFM images of MMT-BR-5, the MMT surface was covered mainly by irregular aggregates, while particulate structures were rarely observed. The topography of the surface was investigated by AFM, and representative phase images of  $1.0 \mu\text{m} \times 1.0 \mu\text{m}$  scans were displayed in Figures 7 (a) and (b). From the height profile analysis of the image, it can be observed that the average height and RMS roughness of the MMT and MMT-BR-5 are found to be 5.50  $\mu\text{m}$  and 723.19 nm, respectively and are illustrated in Table 4 along with all other morphological parameters. However, in the case of MMT these are obtained as 723.19 nm and 70.35 nm, which are significantly smaller than those in the MMT-BR-5. Thus, it can be said that the roughness and the average height of film were increased after the incorporation of dye molecules in the MMT. These observations confirm the formation of nano-dimensional organic-inorganic hybrid molecular assemblies on a solid support. However, as the dimension of the dye molecules are so small compared to size of clay it is very hard to differentiate the two

AFM images visually. Besides, MMT and BR-5 molecules are not distinguishable because their dimensions are beyond the resolution of the AFM instrument (Chakraborty et al., 2017).

### 3.2. PRELIMINARY EXPERIMENTS OF BR-5 ADSORPTION ON MMT

Initially, the optimum conditions for maximum adsorption of the on MMT samples were investigated. For this purpose, the amount of MMT, pH, concentration of the BR-5, time and temperature were changed over a wide range.

Figure 8 shows the effect of the amount of MMT dosage on the BR-5 removal. MMT samples were stirred with 100 mL of 50 mg/L BR-5 solution for different MMT amounts for 60 min. As it can be seen from Figure 8, with the increase of adsorbent dosage, the removal efficiency of BR-5 increased, too. The removal efficiency increased from 60.00 % to 100.00 % for an increase in the adsorbent dosage from 0.10 g/L to 2.0 g/L. According to the results, optimum MMT dosage was found as 0.50 g/L and removal efficiency was 92.76 %.

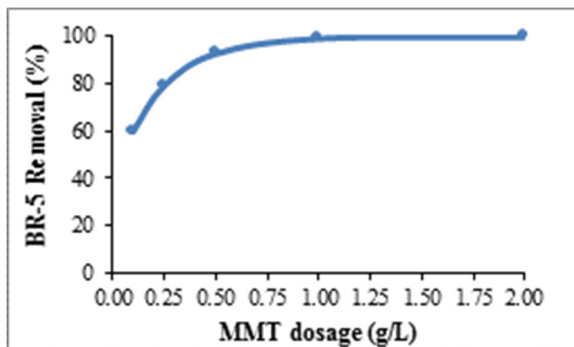


Fig. 8 Effect of MMT dosage on the removal of BR-5 ( $C_0$ :50 mg/L, stirring time: 60 min).

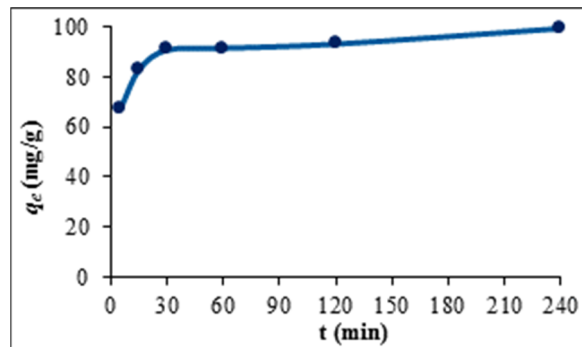


Fig. 9 Effect of contact time on the adsorption of BR-5 by MMT ( $C_0$ :50 mg/L,  $m$ :0.50 g/L).

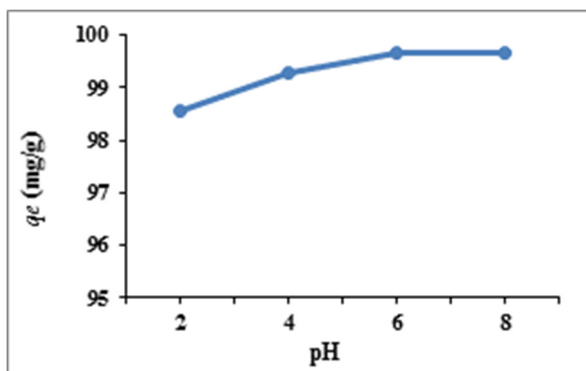


Fig. 10 Adsorption capacity versus different pH values ( $C_0$ :50 mg/L;  $m$ :0.50 g/L; stirring time: 60 min).

Figure 9 shows the effect of contact time on the adsorption capacity. The adsorption capacity of MMT for BR-5 increased gradually with the contact time, reaching nearly 99.31 % at 240 min. A very rapid initial adsorption over 30 min, followed by a longer period of considerably slower uptake, reached equilibrium in 60 min. Optimum contact time to attain equilibrium with MMT was found to be 60 min, and removal efficiency was found to be 91.43 % in 60 min.

### 3.2.1. EFFECT OF PH AND SURFACE CHARGE OF MMT

The effect of pH on BR-5 removal efficiency of MMT was investigated (Fig. 10) at a constant initial concentration (50 mg/L), adsorbent dosage (0.5 mg/L), and contact time (60 min). The adsorption capacity increased as the initial pH increased from 2 to 8. In different pH ranges, the behaviour of MMT can be explained by its surface properties. The adsorption ability of the clay surfaces and the type of surface-active centers are indicated by the significant factor that is the point of zero charge ( $pH_{pzc}$ ). The pH at which the surface charge is zero is called the point of zero charge (pzc) and is typically used to quantify or define the electrokinetic properties of a surface. According to the literature data, however, it is rather difficult to determine an absolute point of zero charge (pzc) for the clays (Errais et al., 2012).

MMT does not have a  $pH_{pzc}$ , and zeta potential studies showed that the surface is negatively charged throughout the whole pH-range, with negative charges increasing further as the pH changes from acidic to the basic range. When the behaviour of the suspensions prepared with MMT at different pH values is examined, the pH of the suspension adjusted to 3 rises to 8 within 15 minutes. The pH of the suspension adjusted to pH value of 11 reached 9.5 equilibrium pH within 2 hours. Therefore, it is difficult to work with MMT at different pH. BR-5 has pH dependent structural equilibrium between the protonated form (acid form) and alkanolamine form (neutral form) with a  $pK_a$  6.8 (Shang et al., 2007; Chang et al., 2016; Sarma et al., 2016; Huang et al, 2017; Hamza et al., 2018).

At the low pH values, the surface of MMT is protonated, and the adsorption mainly takes place with the ion exchange between BR-5 and  $H^+/Na^+$  on MMT's surface. The interlayer negative charges of the MMT minerals are likely to be the host to the cationic dye species (Bhattacharyya et al., 2014).

At the high pH values, the surface of MMT becomes negatively charged due to the deprotonation process, which enhances the adsorption of the positively charged BR-5 molecule through electrostatic attraction. As a result, BR-5 molecules are closely adsorbed onto the surface of MMT, which leads to the formation of BR-5–MMT equilibrium. Besides, more surface aluminol and silanol groups are dissociated at high pH values, which can provide more available adsorption sites for binding BR-5 (Wu et al., 2011; Ijagbemi et al., 2009).

### 3.2.2. ADSORPTION MECHANISM, CATION EXCHANGE CAPACITIES AND EXCHANGE CATIONS

According to the structure of MMT (T.O.T or 2:1) the adsorption of the BR-5 molecules can be described by two mechanisms. (i) pH-independent adsorption generally attributed to cation exchange in the interlayers resulting from electrostatic interactions between ions and negative permanent charge. This situation arises from isomorphic replacement of  $Al^{3+}$ , by  $Mg^{2+}$  or  $Fe^{2+}$  in the octahedral layer. (ii) pH-

dependent adsorption, which results from surface complexation reactions and uses the silanol (Si-OH) and aluminol (Al-OH) sites located at the edges of the layer (Benhammou et al., 2005). MMT has two siloxane tetrahedral sheets sandwiching an aluminum octahedral sheet. Because of the isomorphous substitution within the layers (e.g.,  $\text{Al}^{3+}$  replaced by  $\text{Mg}^{2+}$  or  $\text{Fe}^{2+}$  in the octahedral sheet and  $\text{Si}^{4+}$  replaced by  $\text{Al}^{3+}$  in the tetrahedral sheet), the clay layers have permanent negative charges, which must be counterbalanced by exchangeable cations such as  $\text{Na}^+$  and  $\text{Ca}^{2+}$  in the interlayer. The content of exchangeable cations can be expressed as cation exchange capacity (CEC). The cation-exchange capacity (CEC) of MMT was found 50 mmol/100 g by methylene blue method (Calábria et al., 2013; Turkoz and Tosun, 2011). The interlayer negative charges of the MMT minerals are likely to be the host to the cationic dye species. Due to its unique structure, MMT can be modified easily and then has wide applications in many fields, which have attracted a great deal of interest. The cation exchange capacity of MMT increases the adsorption capacity due to the described ion exchange (Bhattacharyya et al., 2014; Sankin et al., 2014). The adsorption BR-5 on MMT is attributed to ion exchange reaction of BR-5 molecules with the coexisting cation under the experimental conditions.

### 3.3. ADSORPTION ISOTHERMS

The adsorption isotherm models are determined to describe the interaction between the adsorbate and adsorbent. The experimental data are tested with respect to Langmuir, Freundlich, Temkin, Dubinin-Radushkevich, Harkins-Jura, Flory Huggins and Scatchard isotherm models. All relative parameters of the isotherm equations and the determined coefficients ( $R^2$ ) are listed in Table 5.

The Langmuir isotherm models indicate that the adsorption of Basic Red-5 is characterized by monolayer coverage of adsorbate molecules on the adsorbent outer surface. This isotherm model shows that the adsorptive forces are similar to the forces in the chemical interaction.  $q_m$  and  $k_L$  are the Langmuir constants related to the adsorption capacity (mg/g) and equilibrium constant (L/g), respectively. The Langmuir monolayer adsorption capacity ( $q_m$ ) gives the amount of the dye required to occupy all the available sites per unit mass of the sample. The Langmuir monolayer adsorption capacity of BR-5 was estimated as 163.93 mg/g (Table 5) (Brdar et al., 2012; Ijagbemi et al., 2009; Tabak et al., 2009). Freundlich isotherm describes on the surface heterogeneity and exponential distribution of the active sites and their energies. Freundlich parameters are  $n$  and  $k_F$ . In the adsorption processes,  $n$  value was found as 7.50. This value indicates that the adsorption intensity is favourable over the entire range of concentrations studied.

The Temkin isotherm explains how to have the effect of some indirect adsorbate/adsorbent interaction

on the adsorption. Also, the heat of adsorption of all the molecules in the layer would decrease linearly with coverage. In this model,  $T$  the absolute temperature in  $K$  and  $R$  is the universal gas constant, 8.314 J/mol K.  $a_T$  and  $b_T$  is related to the heat of adsorption.

The Dubinin-Radushkevich (D-R) isotherm is related to the porous structure of the sorbent. D-R isotherm is an analogue of Langmuir isotherm. It describes the adsorption on a single type of uniform pores. This isotherm is more general than the Langmuir isotherm because it does not assume a homogenous surface or constant sorption potential. The linear form of D-R isotherm model is given in Table 5. The D-R parameter  $\epsilon$  is the Polanyi potential, which can be calculated through Eq. 3.

$$\epsilon = RT \ln\left(1 + \frac{1}{C_e}\right) \quad (\text{Eq. 3})$$

D-R constant  $K$  is related to the mean free energy of adsorption when it is transferred to the solid form infinity in the solution. The mean adsorption energy  $E$  can be calculated by the Eq (4).

$$E = (-2K)^{-0.5} \quad (\text{Eq. 4})$$

The values of  $E$  arranged as  $E > 8$  kJ/mol and  $E < 8$  kJ/mol propose that the adsorption interaction is chemical or physical, respectively (Brdar et al., 2012; Han et al., 2008). According to Table 5,  $E$  value was found 12.127 kJ/mol, which indicates that chemical interaction played a significant role in the adsorption of Basic Red-5 onto MMT.

Harkins-Jura gives the best agreement with equilibrium data in the case of three-parameter multilayer adsorption isotherm models. Especially at high concentrations, that the high fit of adsorption data to Harkins-Jura equations, which account for multilayer adsorption, can be explained with the existence of heterogeneous pore distribution.  $A$  and  $B$  are Harkins-Jura adsorption constants and their values are given in Table 5 (Basar, 2006; Kaveeshwar et al., 2018).

Flory-Huggins isotherm model, which occasionally derives from the degree of surface coverage characteristics of adsorbate onto adsorbent, can express the feasibility and spontaneous nature of the adsorption process.  $\theta = 1 - C_e/C_0$  is the degree of surface coverage;  $k_{FH}$  is the Flory-Huggins model equilibrium constant and  $n_{FH}$  the Flory-Huggins model exponent (Vijayaraghavan et al., 2016). The Flory-Huggins isotherm model equations were expressed by  $\frac{\theta}{C_e} = k_{FH}(1 - \theta)^{n_{FH}}$  and  $\theta = \left(1 - \frac{C_e}{C_0}\right)$ . There is not a  $q_e$  parameter in this model. Therefore,  $q_e$  values could not be calculated for  $C_e$  values and were not shown in Figure 12.

Scatchard analysis is widely used to investigate the characteristics of the adsorption process since it offers an intuition about the characteristics of the isotherm in a simple manner.  $q_e$  and  $C_e$  are the equilibrium BR-5 adsorption capacity of the MMT and the equilibrium BR-5 concentration in the aqueous



**Table 5** The results of adsorption isotherm models of BR-5 via MMT.

Isotherm models	Equation	Parameters	R <sup>2</sup>
Langmuir	$\frac{C_e}{q_e} = \frac{1}{kq_m} + \frac{1}{q_m} C_e$	$q_m$ (mg/g) $k_L$ (L/mg)	163.930 0.977
Freundlich	$\ln q_e = \ln k + \left(\frac{1}{n}\right) \ln C_e$	$n$ $k_F$ ((mg/g) (L/mg) <sup>1/n</sup> )	7.500 88.898
Temkin	$q_e = \left(\frac{RT}{b_T}\right) \ln a_T + \left(\frac{RT}{b_T}\right) (\ln C_e)$	$a_T$ (L/mg) $b_T$ (kJ/mol)	10710 10.69
Dubinin-Radushkevich	$\ln q_e = K \varepsilon^2 + \ln q_{DR}$	$q_{DR}$ (mg/g) $E$ (kJ/mol) $K$ (mol <sup>2</sup> /kJ <sup>2</sup> )	104.063 12.90 0.0034
Harkins-Jura	$\frac{1}{q_e^2} = \left(\frac{B}{A}\right) - \left(\frac{1}{A}\right) \log C_e$	$A$ (g <sup>2</sup> /L) $B$ (mg <sup>2</sup> /L)	10000 2.000
Flory Huggins	$\frac{\theta}{C_e} = k_{FH}(1 - \theta)^{n_{FH}}$	$k_{FH}$ (L/g) $n_{FH}$	28.424 -17.398
Scatchard	$\frac{q_e}{C_e} = k_s(q_m - q_e)$	$q_m$ (mg/g) $k_s$ (L/mg)	129.766 235.16

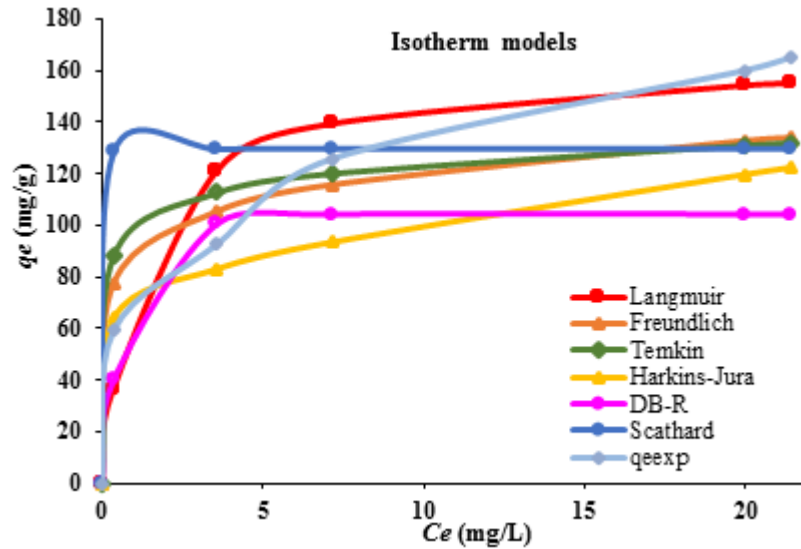


**Fig. 11** Effect of initial concentration and adsorption isotherms of the of BR-5 onto MMT.

solution, respectively, and  $q_m$  (mg/g) and  $k_s$  (L/mg) are the adsorption isotherm parameters (Zheng et al., 2016).

The isotherm model equations and their parameter values are given in Table 5 and Figure 11 (Kiransan et al., 2014; Rezakazemi and Shirazian, 2019).

In Table 6, the adsorption capacity determined from the Langmuir model onto MMT was compared with the other adsorbents. It is seen from the table that MMT has an excellent adsorption capacity with 163.93 mg/g when compared with natural adsorbents, except for the spent cottonseed hull substrate. Only for spent cottonseed hull substrate, the adsorption capacity was higher than MMT. However, some synthesized adsorbents also gave good results from

MMT. These are titanium peroxide powder, Zn<sub>3</sub>[Co(CN)<sub>6</sub>]<sub>2</sub>.nH<sub>2</sub>O nanospheres, Typha orientalis carbon-Mn(NO<sub>3</sub>)<sub>2</sub>, modified cetylpyridinium bromide hectorite and Mesoporous carbon spheres. The preparation of these adsorbents is expensive and time-consuming. Therefore, it cannot be recommended for use in the treatment of dye wastewaters. Compared to other adsorbents, raw MMT can be recommended as a highly suitable adsorbent for BR-5 and cationic dye removal.

**3.4. KINETIC STUDIES**

Adsorption kinetics models explain the adsorption mechanism and the potential rate-controlling steps involved in the process of adsorption. In this study, pseudo-first-order, pseudo-second-order,

**Table 6** Comparison of adsorption capacity ( $q_m$ ) for the adsorption of BR-5 by different adsorbents.

Adsorbents	BR-5	$q_m$ (mg/g)	References
MMT	BR-5	163.93	This study
Spent cottonseed hull substrate	BR-5	166.70	Qi et al. (2011)
Peanut husk	BR-5	37.46	Han et al. (2008)
Sawdust	BR-5	72.46	Elhami et al. (2012)
Bagasse	BR-5	123.46	Elhami et al. (2012)
Titanium peroxide powder	BR-5	327.61	Zhao et al. (2014)
Zn <sub>3</sub> [Co(CN) <sub>6</sub> ] <sub>2</sub> .nH <sub>2</sub> O nanospheres	BR-5	232.56	Wang et al. (2013)
Polydopamine microspheres	BR-5	123.76	Fu et al. (2016)
Fe <sub>3</sub> O <sub>4</sub> hollow nanospheres	BR-5	105.00	Iram et al. (2010)
Magnetic multi-wall carbon nanotube	BR-5	9.81	Gong et al. (2009)
<i>Typha orientalis</i> carbon-Mn(NO <sub>3</sub> ) <sub>2</sub>	BR-5	190.08	Zhang et al. (2008)
Modified cetylpyridinium bromide hectorite	BR-5	393.70	Yue et al. (2011)
Halloysite nanotubes	BR-5	54.85	Luo et al. (2010)
Mesoporous carbon spheres	BR-5	204.50	Tian et al. (2015)

**Table 7** The kinetics constants for the removal of the BR-5 by MMT.

Kinetic models	Equation	Parameters	R <sup>2</sup>
Pseudo-first-order	$\ln(q_e - q_t) = \ln q_e - k_1 t$	$q_e$ (mg/g) $k_1$ (min <sup>-1</sup> )	16.940 0.0574
Pseudo-second-order	$\frac{t}{q_t} = \frac{1}{k_2 q_e^2} + \frac{1}{q_e} t$	$q_e$ (mg/g) $k_2$ (g/mg.min)	100.000 0.0024
Intra-particle diffusion	$q_t = k_{dif} t^{1/2} + C$	$k_{dif}$ (mg/g.min <sup>1/2</sup> ) $C$	1.923 72.758
Elovich	$\ln q_e = \frac{1}{T} \ln(\alpha T) + \frac{1}{T} \ln t$	$T$ (g/mg.min) $\alpha$ (mg.min <sup>2</sup> /g)	0.132 20 952.220

intraparticle diffusion and Elovich models are studied for describing the mechanism and the potential rate-controlling steps involved in the process of adsorption. The contact time was studied between 5 and 240 min. (5, 15, 30, 60, 90, 120, 240 min.). For this study, different kinetic models were analyzed, and the results were given in Table 7.

Pseudo-first-order model equations were given in Table 7 where  $q_e$  and  $q_t$  are the adsorption capacities at the time  $t$  and at equilibrium, respectively (mg/g),  $k_1$  (min<sup>-1</sup>) is the rate constant of pseudo-first-order adsorption, and  $t$  is the contact time (min).

Pseudo-second-order model differential equations were given in Table 7 where  $q_e$  and  $q_t$  are the adsorption capacities at the time  $t$  and at equilibrium, respectively (mg/g),  $k_2$  (g/mg.min) is the rate constant of pseudo-second-order adsorption, and  $t$  (min) is the contact time.

The rate parameter for the intra-particle diffusion equation was given in Table 7 where  $C$  is the intercept and  $k_{dif}$  (mg/g.min<sup>1/2</sup>) is the intra-particle diffusion constant.

The rate parameter for Elovich equation was given in Table 7 where  $\alpha$  (mg.min<sup>2</sup>/g) and  $T$  (g/mg.min) are the equilibrium rate constants for Elovich model.

The value of calculated  $q_{e,cal}$  in the case of the pseudo-second-order model, is very close to the experimental value for dye initial concentration. For example, when the initial concentration of BR-5 was 50 mg/L and temperature 22 °C, the experimental  $q_{e,exp}$  was 91.43 mg/g whereas the calculated values of  $q_{e,cal}$  were 16.94, 100.00, 78.84 and 91.052 mg/g for pseudo-first-order, pseudo-second-order, intra-particle diffusion models and Elovich, respectively.

The correlation coefficients were given in Table 6 for kinetic models. According to the results, the kinetic data gave the best fit with the pseudo-second-order model, as shown by the high correlation coefficients. Figure 12 shows the linear plots of  $t/q_t$  versus  $t$ . The correlation coefficient for the pseudo-second-order kinetic model was found as 0.99. This result indicates the applicability of this kinetic model of the adsorption process of BR-5 on MMT. Similar results have been crystal violet (Eren and Afsin, 2009) and congo red (Namasivayam and Kavitha, 2002).

### 3.5. EFFECT OF TEMPERATURE AND THERMODYNAMIC PARAMETERS

The thermodynamic parameters for the adsorption process are  $\Delta H^\circ$ ,  $\Delta S^\circ$  and  $\Delta G^\circ$ . These parameters were determined from the experimental

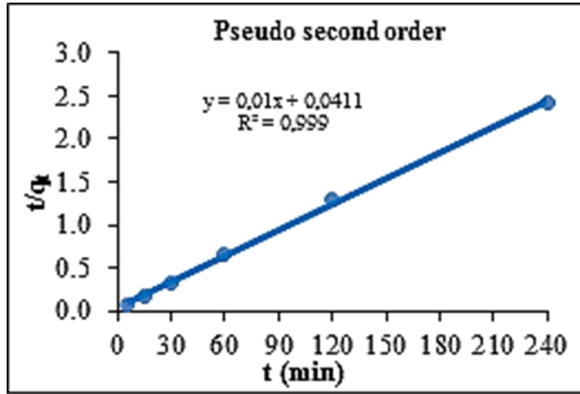


Fig. 12 Linerized pseudo-second-order kinetics plots for BR-5 adsorption ( $T= 22\text{ }^{\circ}\text{C}$ ,  $C_0$ : 50 mg/L, dosage: 0.5g/L).

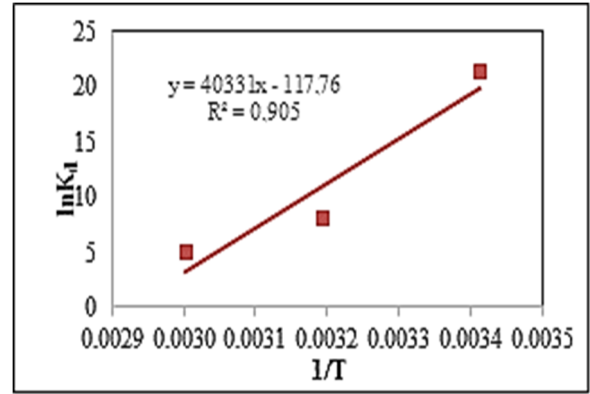


Fig. 13 Plot of  $\ln K_d$  versus  $1/T$  for BR-5.

Table 8 Thermodynamic parameters for adsorption of BR-5 by MMT.

Initial concentration (mg/L) BR-5	$\Delta H^{\circ}$ (kJ/mol)	$\Delta S^{\circ}$ (kJ/mol K)	$\Delta G^{\circ}_{293K}$ (kJ/mol)	$\Delta G^{\circ}_{313K}$ (kJ/mol)	$\Delta G^{\circ}_{333K}$ (kJ/mol)
50.00	-0.979	-335.311	-300.800	-298.450	-296.097

Table 9 Design matrix and the results of the  $2^3$  full factorial design.

Run No.	Factor			$q_e$ (mg/g)		
	A	B	C	Replicate		Average
				I	II	
1	-1	-1	-1	92.85	91.20	92.03
2	+1	-1	-1	160.00	159.20	159.60
3	-1	+1	-1	91.44	93.38	92.45
4	+1	+1	-1	181.44	180.20	180.82
5	-1	-1	+1	49.65	47.28	48.47
6	+1	-1	+1	98.57	99.36	98.97
7	-1	+1	+1	37.86	35.98	36.92
8	+1	+1	+1	93.93	91.78	92.86

data: (Erdem et al., 2004; Tabak et al., 2009) (Eqs. 5, 6, 7):

$$K_d = q_e/C_e \quad (\text{Eq.5})$$

$$\Delta G^{\circ} = \Delta H^{\circ} - T\Delta S^{\circ} \quad (\text{Eq.6})$$

$$\ln K_d = \frac{\Delta S^{\circ}}{R} + \frac{\Delta H^{\circ}}{RT} \quad (\text{Eq.7})$$

where  $K_d$  (mL/g) is the distribution coefficient for adsorption,  $R$  is the gas constant ( $8.314 \times 10^{-3}$  kJ/Kmol),  $\Delta H^{\circ}$  (kJ/mol),  $\Delta S^{\circ}$  (kJ/mol K) and  $\Delta G^{\circ}$  (kJ/mol) are the changes of enthalpy, entropy and the Gibbs energy, respectively.  $q_e$  and  $C_e$  are adsorption capacity and equilibrium concentrations of BR-5 in solution, respectively. The enthalpy change ( $\Delta H^{\circ}$ ) and the entropy change ( $\Delta S^{\circ}$ ) can be calculated from a plot of  $\ln K_d$  versus  $1/T$  (Fig. 13; Eren and Afsin, 2009).

Calculated values of thermodynamic parameters are given in Table 8. As indicated by  $\Delta H^{\circ}$  value, the adsorption of BR-5 on MMT was exothermic.

The negative values of entropy ( $\Delta S^{\circ}$ ) change suggest no structural changes in adsorbate and adsorbent. The negative free energy ( $\Delta G^{\circ}$ ) changes are between -296.077 and -300.800 kJ/mol for MMT. The nature of the adsorption process is spontaneous due to the negative values of  $\Delta G^{\circ}$ . The negative  $\Delta S^{\circ}$  values show decrease randomness at the MMT/BR-5 interface. This situation suggests that no significant changes occur in the internal structure of the adsorbent by the adsorption of BR-5 onto MMT. The adsorption process indicated that the adsorption capacity increased with the increase of temperature.

### 3.6. FACTORIAL EXPERIMENTAL DESIGN

The results of factorial design experiments were given (initial concentration, time and dosage) for adsorption in Table 9. The response variable was selected as the adsorption capacity. All possible combinations of the variables were created, and the experiments were performed in duplicates.

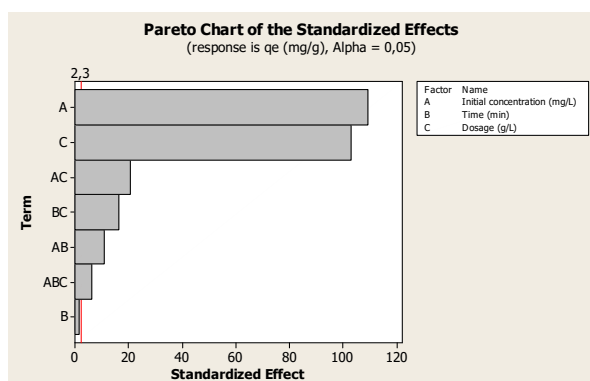
**Table 10** Estimated effects and coefficients for  $q_e$ .

Term	Effect	Coef	SE Coef	T	P
Constant		100.26	0.3001	334.04	0.000
A	65.60	32.80	0.3001	109.29	0.000
B	0.99	0.49	0.3001	1.65	0.139
C	-61.91	-30.96	0.3001	-103.14	0.000
A*B	-6.57	3.28	0.3001	10.94	0.000
A*C	-12.39	-6.19	0.3001	-20.64	0.001
B*C	-9.81	-4.91	0.3001	-16.35	0.000
A*B*C	-3.85	-1.92	0.3001	-6.41	0.000

S = 1.20056 R-Sq = 99.97 % R-Sq(pred) = 99.86 % R-Sq(adj) = 99.94 %

**Table 11** Analysis of variance.

Source	Degree of Freedom	Sum of squares (SS)	Mean squares (SS)	F	P
Main effects	3	32552.6	32552.6	7528.27	
A	1	17216.1	17216.1	11944.40	0.000
B	1	3.9	3.9	2.71	0.139
C	1	15332.6	15332.6	10637.69	0.000
AB	1	1171.7	1171.7	119.70	0.000
AC	1	613.8	613.8	425.85	0.000
BC	1	385.3	385.3	267.34	0.000
ABC	1	59.3	59.3	41.14	0.000
Residual Error	8	11.5	11.5		
Pure Error	8	11.5	11.5		
Total	15	33795.1			

**Fig. 14** Pareto chart of standardized effects on  $q_e$ .

According to the results of Table 10, the model equation was derived by using the regression coefficient. The empirical model for the adsorption capacity ( $q_e$ ) can be given as:

$$q_e = 100.26 + 32.80A + 0.49B - 30.96C + 3.28AB - 6.19AC - 4.91BC - 1.92ABC \quad (\text{Eq. 8})$$

Except from B, the effects of all other factors have significant at 95 % confidence level.  $R^2$  (99.97 %) and  $R_{\text{adj}}^2$  (99.94 %) values indicate that the empirical model was successful in correlating to the parameters (Table 10).

### 3.6.1. STUDENT'S T-TEST

Student's  $t$ -test was applied to determine the significance of numerical values of effects, coefficient, standard error, T and P (Table 10). The P values of less than 0.05 indicate that model terms are significant. The Pareto chart shows the relative importance of the individual and interaction effects (Figure 14). By having a confidence level of 95 % and sixteen degree of freedom,  $t$ -value can be seen as 2.3 in Figure 14.

### 3.6.2. ANALYSIS OF VARIANCE (ANOVA)

The main and interaction effects of factors were displayed in Table 11. According to the results  $F$ -ratio and P-value, it is observed that the effects of initial concentration (A) and dosage (C), and the interaction effect of initial concentration and time ( $A \times B$ ), initial concentration and dosage ( $A \times C$ ), time and dosage ( $B \times C$ ), initial concentration, time and dosage ( $A \times B \times C$ ) are statistically significant. According to the interaction effects and factors reduced model equation was given to the following equation.

$$q_e = 100.26 + 32.80A - 30.96C + 3.28AB - 6.19AC - 4.91BC - 1.92ABC \quad (\text{Eq. 9})$$

This empirical model was carried out to eliminate the effects of insignificant factors. In order to suggest an appropriate model, the significant interaction and main effects of factors were studied with an analysis of variance (ANOVA). The results were given in Table 11. The determined  $F$ -value and

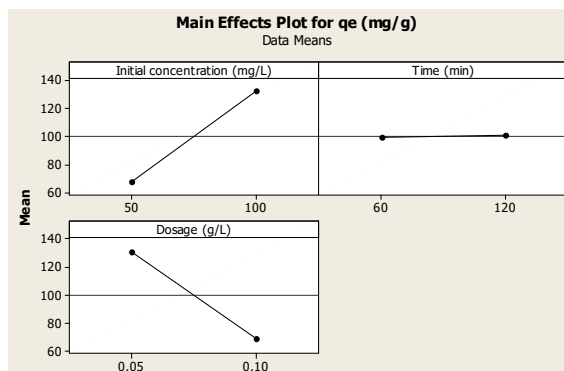


Fig. 15 Main effects plot for  $q_e$ .

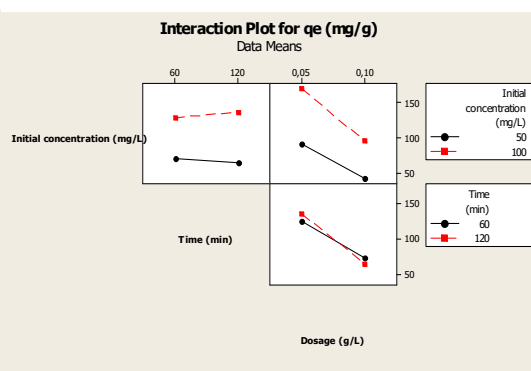


Fig. 16 Interaction graphs for  $q_e$ .

$P$ -value less than 0.05 indicate a very well fit for the model of experimental data at 95 % confidence level.

### 3.6.3. THE MAIN AND INTERACTION EFFECTS

The main effect graphs of parameters on the adsorption process are shown in Figure 15. The main effects of parameters are explained effects on adsorption process and represent deviations of an average between the high and low levels for each one of them (Abdel-Ghani et al., 2009; Ponnusami et al., 2007). The positive effect on the response variable,  $q_e$ , are determined to the factor changes from low to high levels. On the other hand, the negative effect on the  $q_e$  is determined to the factor changes from high to low levels (Lee et al., 2006). It can be seen that the initial concentration ( $A$ ) has a strong positive effect, time ( $B$ ) has mild effect and dosage ( $C$ ) has a strong negative effect on the adsorption processes. According to the Eq. 9, initial concentration ( $A$ ) has a high positive effect.

In order to explain the interaction effects between experimental parameters, interaction effects graphs were shown in Figure. 16. The non-parallel lines in the graphs indicate the interaction between two parameters. Interaction graphs (Figure 16) and equation 9 showed a positive interaction between initial concentration and time ( $AB$ ), and negative interaction between initial concentration and dosage ( $AC$ ) and time and dosage ( $BC$ ).

## 4. CONCLUSION

The morphological structure and composition of MMT were characterized by X-RD, X-RF, FT-IR, SEM-EDS, AFM, TGA and DSC analysis. For the characterization of this local MMT, FTIR, DSC, TGA and AFM techniques were used for the first time. In addition, the agglomeration properties were determined by AFM with cross-section analysis. Adsorption properties of the MMT were investigated by depending on various adsorption conditions such as different initial dye concentrations, contact times, adsorbent dosage, pH and temperature. Seven isotherm models were studied in determining the adsorption capacity of MMT for the BR-5. The

Langmuir isotherm model was found to be in a good fit with the equilibrium adsorptions. The maximum adsorption capacity is 163.93 mg/g.

For modeling the adsorption mechanism of the BR-5 onto MMT, four kinetic models were used. The pseudo-second-order kinetic model was found to be more suitable than the higher correlation coefficient ( $R^2=99.97\%$ ) of other models. After the equilibrium adsorption time of 60 min, the adsorption capacity for BR-5 reaches about 100.0 mg/g and  $>98\%$  efficiency.

$\Delta G^\circ$  values changed from -300.80 to -296.09 kJ/mol when temperature range 293-333 K. The thermodynamic values show that the adsorption process is exothermic and the process will proceed spontaneously.

The factorial design is applied successfully to determine the effects of adsorption parameters, and the  $R^2$  value was found as 99.97 %. The adsorption capacity of MMT is found very effective compared to the other adsorbents. The results of the present study demonstrated that MMT is a cheap and suitable adsorbent that can be used directly for the removal of cationic dye from aqueous solutions.

## ACKNOWLEDGMENTS

This study was supported by Ondokuz Mayıs University PYO.MUH.1904.15.018 project number.

## REFERENCES

- Abdel-Ghani, N.T.C.: 2009, Factorial experimental design for biosorption of iron and zinc using *Typha domingensis* phytomass. *Desalination*, 249, 343–347. DOI: 10.1016/j.desal.2009.02.065
- Ates, G., Vanhaecke, T., Rogiers, V. and Rodrigues, R.M.: 2017, Assaying cellular viability using the neutral red uptake assay. *Methods Mol. Biol.*, 1601, 19–26. DOI: 10.1007/978-1-4939-6960-9-2
- Basar, C.A.: 2006, Applicability of the various adsorption models of three dyes adsorption onto activated carbon prepared waste apricot. *J. Hazard. Mater.*, B135, 232–241. DOI: 10.1016/j.jhazmat.2005.11.055
- Benhammou, A., Yaacoubi, A., Nibou, L. and Tanotti, B.: 2005, Adsorption of metal ions onto Moroccan

- stevensite: kinetic and isotherm studies. *J. Colloid Interface Sci.*, 282, 320–326.  
DOI: 10.1016/j.jcis.2004.08.168
- Bergaya, F. and Lagaly, G.: 2008, General introduction: clays and clay minerals, and clay science. *Handbook of Clay Science*, Dev. Clay Sci., 1.  
DOI: 10.1016/S1572-4352(05)01001-9
- Bhattacharyya, K.G., Sen-Gupta, S. and Sarma, G.K.: 2014, Interactions of the dye, Rhodamine B with kaolinite and montmorillonite in water. *Appl. Clay Sci.*, 99, 7–17. DOI: 10.1016/j.clay.2014.07.012
- Brdar, M., Sciban, M., Takaci, A. and Dosenovic, T.: 2012, Comparison of two and three parameters adsorption isotherm for Cr(VI) onto Kraft lignin. *Chem. Eng. J.*, 183, 108–111. DOI: 10.1016/j.ccej.2011.12.036
- Bujdak, J.: 2006, Effect of the layer charge of clay minerals on optical properties of organic dyes. A review. *Appl Clay Sci.*, 34, 58–73.  
DOI: 10.1016/j.clay.2006.02.011
- Calábria, J.A.A., Amaral, D.N., Ladeira, A.C.Q., Cota, S.D.S. and Silva, T.S.S.: 2013, Determination of the cation exchange capacity of bentonite exposed to hyperalkaline fluid. *International Nuclear Atlantic Conference – INAC. Brazil*.
- Chakraborty, U., Singha, T., Chianelli, R.R. and Hansda, C.: 2017, Organic-inorganic hybrid layer-by-layer electrostatic self-assembled film of cationic dye Methylene Blue and a clay mineral: Spectroscopic and Atomic Force microscopic investigations. *J. Lumin.*, 187, 322–332. DOI: 10.1016/j.jlumin.2017.03.039
- Chang, J., Ma, J., Ma, Q., Zhang, D., Qiao, N., Hu, M. and Ma, H.: 2016, Adsorption of methylene blue onto Fe<sub>3</sub>O<sub>4</sub>/activated montmorillonite nanocomposite. *Applied Clay Science*, 119, 132–140.  
DOI: 10.1016/j.clay.2015.06.038
- Djomgoue, P. and Njopwouo, D.: 2013, FT-IR spectroscopy applied for surface clays characterization. *J. Surf. Eng. Mater. Adv. Technol.*, 3, 275–282.  
DOI: 10.4236/jsemat.2013.34037
- Elhami, S., Faraji, H. and Taheri, M.: 2012, Removal of neutral red dye from water samples using adsorption on bagasse and sawdust. *J. Chem. Soc. Pak.*, 34, 2, 269–272.
- Eren, E.: 2009, Investigation of a basic dye removal from aqueous solution onto chemically modified Unye bentonite. *J. Hazard. Mater.*, 166, 88–93.  
DOI: 10.1016/j.jhazmat.2008.11.011
- Erdem, E., Karapinar, N. and Donat, R.: 2004, The removal of heavy metal cations by natural zeolites. *J. Colloid Interf. Sci.*, 280, 309–314.  
DOI: 10.1016/j.jcis.2004.08.028
- Eren, E. and Afsin, B.: 2009, Removal of basic dye using raw and acid activated bentonite samples. *J. Hazard. Mater.*, 166, 830–835.  
DOI: 10.1016/j.jhazmat.2008.11.132
- Errais, E., Duplay, J., Elhabiri, M., Khodja, M., Ocampo, R., Baltenweck-Guyot, R. and Darragi, F.: 2012, Anionic RR120 dye adsorption onto raw clay: Surface properties and adsorption mechanism. *Colloids Surf. A Physicochem. Eng. Asp.*, 403, 69–78.  
DOI: 10.1016/j.colsurfa.2012.03.057
- Farooq, S., Saeed, A., Sharif, M., Hussain, J., Mabood, F. and Iftekhar, M.: 2017, Process optimization studies of crystal violet dye adsorption onto novel, mixed metal Ni<sub>0.5</sub>Co<sub>0.5</sub>Fe<sub>2</sub>O<sub>4</sub> ferrosinell nanoparticles using factorial design. *J. Water Process Eng.*, 16, 132–141.  
DOI: 10.1016/j.jwpe.2017.01.001
- Fotakis, G. and Timbrell, J.A.: 2006, In vitro cytotoxicity assays: comparison of LDH, neutral red, MTT and protein assay in hepatoma cell lines following exposure to cadmium chloride. *Toxicol. Lett.*, 160, 2, 171–178. DOI: 10.1016/j.toxlet.2005.07.001
- Földvári, M.: 2011, Handbook of thermogravimetric system of minerals and its use in geological practice. *Occasional Papers of the Geological Institute of Hungary*, 213, Budapest.
- Fu, J., Xin, Q., Wu, Chen, Z., Yan, Y., Liu, S., Wang, M. and Xu, Q.: 2016, Selective adsorption and separation of organic dyes from aqueous solution on polydopamine microspheres. *J. Colloid Interface Sci.*, 461, 292–304.  
DOI: 10.1016/j.jcis.2015.09.107
- Gabor, A., Davidescu, C.M., Negrea, A., Ciopec, M., Grozav, I., Negrea, P. and Duteanu, N.: 2017, Optimizing the lanthanum adsorption process onto chemically modified biomaterials using factorial and response surface design. *J. Environ. Manage.*, 204, 839–844. DOI: 10.1016/j.jenvman.2017.01.046
- Gong, J.L., Wang, B., Zeng, G.M., Yang, C.P., Niu, C.G., Niu, Q.Y., Zhou, W.J. and Liang, Y.: 2009, Removal of cationic dyes from aqueous solution using magnetic multi-wall carbon nanotube nanocomposite as adsorbent. *J. Hazard. Mater.*, 164, 1517–1522.  
DOI: 10.1016/j.jhazmat.2008.09.072
- Gulgonul, I. and Celik, M.S.: 2018, Understanding the flotation separation of Na and K feldspars in the presence of KCl through ion exchange and ion adsorption. *Miner. Eng.*, 129, 41–46.  
DOI: 10.1016/j.mineng.2018.08.038
- Hamza, W., Dammak, N., Hadjtaief, H.B., Eloussaief, M. and Benzina, M.: 2018, Sono-assisted adsorption of Cristal Violet dye onto Tunisian Smectite Clay: Characterization, kinetics and adsorption isotherms. *Ecotox. Environ. Safe*, 163, 365–371.  
DOI: 10.1016/j.ecoenv.2018.07.021
- Han, R.P., Han, P., Cai, Z.H., Zhao, Z.H. and Tang, M.S.: 2008, Kinetics and isotherms of neutral red adsorption on peanut husk. *J. Environ. Sci.*, 20, 1035–1041.  
DOI: 10.1016/S1001-0742(08)62146-4
- Huang, Z.H., Li, Y.Z., Chen, W.J., Shi, J.H., Zhang, N., Wang, X.J., Li, Z., Gao, L.Z. and Zhang, Y.X.: 2017, Modified bentonite adsorption of organic pollutants of dye wastewater. *Mater. Chem. Phys.*, 202, 266–276.  
DOI: 10.1016/j.matchemphys.2017.09.028
- Ijagbemi, C.O., Mi-Hwa, B. and Dong-Su, J.: 2009, MMT surface properties and sorption characteristics for heavy metal removal from aqueous solutions. *J. Hazard. Mater.*, 166, 538–546.  
DOI: 10.1016/j.jhazmat.2008.11.085
- Iram, M., Guo, C., Guan, Y., Ishfaq, A. and Liu, H.: 2010, Adsorption and magnetic removal of neutral red dye from aqueous solution using Fe<sub>3</sub>O<sub>4</sub> hollow nanospheres. *J. Hazard. Mater.*, 181, 1039–1050.  
DOI: 10.1016/j.jhazmat.2010.05.119
- Kaveeshwar, A.R., Ponnusamy, S.K., Revellame, E.D., Daniel, D., Gang, D.D., Zappi, M.E. and Subramaniam, R.: 2018, Pecan shell based activated carbon for removal of iron (II) from fracking wastewater: Adsorption kinetics, isotherm and

- thermodynamic studies. *Process Saf. Environ. Prot.*, 114, 107–122.  
DOI: 10.1016/j.psep.2017.12.007
- Kiransan, M., Soltani, R.D.C., Hassani, A., Karaca, S. and Khataee, A.: 2014, Preparation of cetyltrimethylammonium bromide modified montmorillonite nanomaterial for adsorption of a textile dye. *J. Taiwan Inst. Chem. Eng.*, 45, 2565–2577.  
DOI: 10.1016/j.jtice.2014.06.007
- Lee, C.K., Liu, S.S., Juang, L.C., Wang, C.C., Lyu, M.D. and Hung, S.H.: 2007, Application of titanate nanotubes for dyes adsorptive removal from aqueous solution. *J. Hazard. Mater.*, 148, 756–760.  
DOI: 10.1016/j.jhazmat.2007.07.010
- Lee, I.H., Kuan, Y.C. and Chern, J.M.: 2006, Factorial experimental design for recovering heavy metals from sludge with ion-exchange resin. *J. Hazard. Mater.*, 138, 549–559. DOI: 10.1016/j.jhazmat.2006.05.090
- Lima, L.S., Araujo, M.D.M., Quinária, S.P., Migliorini, D.W. and Garcia, J.R.: 2011, Adsorption modeling of Cr, Cd, and u on activated carbon of different origins by using fractional factorial design. *Chem. Eng. J.*, 166, 881–889. DOI: 10.1016/j.ccej.2010.11.062
- Luo, P., Zhao, Y., Zhang, B., Liu, J., Yang, Y. and Liu, J.: 2010, Study on the adsorption of neutral red from aqueous solution onto halloysite nanotubes. *Water Res.*, 44, 1489–1497.  
DOI: 10.1016/j.watres.2009.10.042
- Mannerström, M., Toimela, T., Sarkanen, J.R. and Heinonen, T.: 2017, Human BJ fibroblasts is an alternative to mouse BALB/c 3T3 cells in In Vitro neutral red uptake assay. *Basic Clin. Pharmacol. Toxicol.*, 3, 121, 109–115. DOI: 10.1111/bcpt.12790
- Namasivayam, C. and Kavitha, D.: 2002, Removal of congo red from water by adsorption on activated carbon prepared from coir pith, an agricultural solid waste. *Dyes Pigm.*, 54, 47–48.  
DOI: 10.1016/S0143-7208(02)00025-6
- Ponnusami, V., Krithika, V., Madhuran, R. and Srivastava, S.N.: 2007, Biosorption of reactive dye using acid-treated rice husk: Factorial design design analysis. *J. Hazard. Mater.*, 142, 397–403.  
DOI: 10.1016/j.jhazmat.2006.08.040
- Qi, Z., Wenqi, G., Chuanxin, X., Dongjiang, Y., Xiaoqing, L., Xiao, Y., Shaohua, C. and Liu, X.: 2011, Removal of neutral red from aqueous solution by adsorption on spent cottonseed hull substrate. *J. Hazard. Mater.*, 185, 502–506. DOI: 10.1016/j.jhazmat.2010.09.029
- Rezakazemi, M. and Shirazian, S.: 2019, Lignin-chitosan blend for methylene blue removal: Adsorption modeling. *J. Mol. Liq.*, 274, 778–791.  
DOI: 10.1016/j.molliq.2018.11.043
- Sanqin, W., Zepeng, Z., Yunhu, W., Libing, L. and Jiansheng, Z.: 2014, Influence of montmorillonites exchange capacity on the basal spacing of cation-anion organo-montmorillonites. *Mater. Res. Bull.*, 59, 59–64. DOI: 10.1016/j.materresbull.2014.06.007
- Sarma, K., Gupta, S.S. and Bhattacharyya, K.G.: 2016, Adsorption of Crystal violet on raw and acid-treated MMT, K10, in aqueous suspension. *J. Environ. Manage.*, 171, 1–10.  
DOI: 10.1016/j.jenvman.2016.01.038
- Shang, L., Zou, X., Jiang, X., Yang, G. and Dong, S.: 2007, Investigations on the adsorption behavior of neutral red on mercaptoethane sulfonate protected gold nanoparticles. *J. Photoch. Photobio. A Chem.*, 187, 152–159. DOI: 10.1016/j.jphotochem.2006.10.008
- Tabak, A., Eren, E., Afsin, B. and Caglar, B.: 2009, Determination of the adsorptive properties of a Turkish Sepiolite for removal of Reactive Blue 15 anionic dye from aqueous solutions. *J. Hazard. Mater.*, 161, 1087–1094. DOI: 10.1016/j.desal.2009.10.020
- Tahir, S.S. and Rauf, N.: 2006, Removal of a cationic dye from aqueous solutions by adsorption onto bentonite clay. *Chemosphere*, 63, 1842–1848.  
DOI: 10.1016/j.chemosphere.2005.10.033
- Tian, Y., Zhong, S., Zhu, X., Huang, A., Chen, Y. and Wang, X.: 2015, Mesoporous carbon spheres: Synthesis, surface modification and neutral red adsorption. *Mater. Lett.*, 161, 656–660.  
DOI: 10.1016/j.matlet.2015.09.055
- Turkoz, M. and Tosun, H.: 2011, The use of methylene blue test for predicting swell parameters of natural clay soils. *Sci. Res. Essays.*, 6, 1780–1792.  
DOI: 10.5897/SRE10.629
- Verissimo, T.V., Santos, N.T., Silva, J.R., Azevedo, R.B., Gomes, A.J. and Lunardi, C.N.: 2016, In vitro cytotoxicity and phototoxicity of surface-modified gold nanoparticles associated with neutral red as a potential drug delivery system in phototherapy. *Mater. Sci. Eng. C.*, 65, 199–204.  
DOI: 10.1016/j.msec.2016.04.030
- Wang, W., Li, C., Yao, J., Zhang, B., Zhang, Y. and Liu, J.: 2013, Rapid adsorption of neutral red from aqueous solutions by  $Zn_3[Co(CN)_6]_2 \cdot nH_2O$  nanospheres. *J. Mol. Liq.*, 184, 10–16.  
DOI: 10.1016/j.molliq.2013.04.018
- Wang, J., Wang, Z., Yang, L., Yang, G., Miao, C. and Lv, P.: 2017, Natural albite as a novel solid basic catalyst for the effective synthesis of biodiesel: Characteristics and performance. *Energy*, 141, 1650–1660.  
DOI: 10.1016/j.energy.2017.11.086
- Wu, X.L., Zhao, D. and Yang, S.T.: 2011, Impact of solution chemistry conditions on the sorption behaviour of Cu(II) on Linan montmorillonite. *Desalination*, 269, 84–91. DOI: 10.1016/j.desal.2010.10.046
- Yeddou-Mezenner, N.: 2010, Kinetics and mechanism of dye biosorption onto an untreated antibiotic waste. *Desalination.*, 262, 251–259.  
DOI: 10.1016/j.desal.2010.06.023
- Yue, D., Jing, Y., Ma, J., Xia, C., Yin, X. and Jia, Y.: 2011, Removal of neutral red from aqueous solution by using modified hectorite. *Desalination*, 267, 9–15. DOI: 10.1016/j.desal.2010.08.038
- Zhao, X., Huang, J., Wang, B., Bi, Q., Dong, L. and Liu, X.: 2014, Preparation of titanium peroxide and its selective adsorption property on cationic dyes. *Appl. Surf. Sci.*, 292, 576–582.  
DOI: 10.1016/j.apsusc.2013.12.011
- Zhang, J., Shi, Q., Zhang, C., Xu, J., Zhai, B. and Zhang, B.: 2008, Adsorption of neutral red onto Mn-impregnated activated carbons prepared from *Typha orientalis*. *Bioresour. Technol.*, 99, 8974–8980.  
DOI: 10.1016/j.biortech.2008.05.018
- Zheng, E., Danga, Q., Liu, C., Fan, B., Yan, J., Yu, Z. and Zhang, H.: 2016, Preparation and evaluation of dipic acid dihydrazide cross-linked carboxymethyl chitosan microspheres for copper ion adsorption. *Colloids Surf. A Physicochem. Eng. Asp.*, 502, 34–43.  
DOI: 10.1016/j.colsurfa.2016.05.003